Void Deformation and Breakup in Shearing Silica Glass

Yi-Chun Chen,[1] Ken-ichi Nomura,[1] Rajiv K. Kalia,[1,2,3] Aiichiro Nakano,[1,2,3] and Priya Vashishta[1,2,3]

[1]*Department of Physics and Astronomy, Collaboratory for Advanced Computing and Simulations, University of Southern California, Los Angeles, California 90089-0242, USA*

[2]*Department of Chemical Engineering and Materials Science, Collaboratory for Advanced Computing and Simulations, University of Southern California, Los Angeles, California 90089-0242, USA*

[3]*Department of Computer Science, Collaboratory for Advanced Computing and Simulations, University of Southern California, Los Angeles, California 90089-0242, USA*

(Received 30 January 2009; published 16 July 2009)

We study shear deformation and breakup of voids in silica glass using molecular dynamics simulations. With an increase in the shear strain, two kinds of defects—threefold-coordinated silicon and nonbridging oxygen atoms—appear as spherical voids deform elastically into ellipsoidal shapes. For shear strains $\varepsilon > 15\%$, nanocracks appear on void surfaces and voids deform plastically into a threadlike structure. Nanocracks are nucleated by the migration of threefold-coordinated Si and nonbridging O on —Si–O–Si–O— rings. For $\varepsilon > 40\%$, the threadlike structures break up into several fragments.

DOI: 10.1103/PhysRevLett.103.035501 PACS numbers: 61.43.Fs, 61.72.Qq, 31.15.xv

Bubble deformation and breakup in sheared viscous fluids is a forefront research area with applications ranging from food processing, ink-jet printing, glass manufacturing, and blending of polymer melts to drug delivery systems and the rheology of magmas [1–4]. Applications of drop deformation and breakup phenomena in fluids span a wide range of spatiotemporal scales. At the continuum level, drop deformation and breakup have been investigated quite extensively [1–3] as a function of the ratio of the drop viscosity ($\lambda\mu$) relative to that of the fluid (μ) and the capillary number $C = \frac{Ga\mu}{\gamma}$, where G is the applied shear rate and a and γ are the drop radius and interfacial tension, respectively. The capillary number represents a competition between shear-flow forces, which tend to deform the drop, and the interfacial tension, which tends to maintain the spherical shape. For a small Reynold's number of fluid motions ($\rho a u/\mu \ll 1$, where ρ and u are the fluid density and velocity, respectively), a spherical drop deforms into an ellipsoid, and the deformation parameter D [$=(L - B)/(L + B)$, where L and B are the length and breadth of the drop, respectively] is proportional to C for $C \ll 1$. As C increases, the drop becomes more elongated and turns into a threadlike structure before breaking up into smaller droplets above a critical value of C [2]. Long, slender shapes are observed for an inviscid drop or a bubble [2], and, in these instances of low viscosity ratios $\lambda \ll 1$, the drop behavior is well described by the slender-body theory [5]. Hinch and Acrivos predicted on the basis of this theory [6] that a spherical bubble under simple shear would deform into an S-shaped, long, thin bubble in the limit $C \to \infty$. Shape measurements on air bubbles in viscous liquids support their prediction, and rheology data on bubble shapes in lava flow at high capillary numbers (rhyolite) also reveal pointed ends on the bubbles [2–4]. Joseph has argued that cavitation in liquids has much in common with crack nucleation in amorphous solids and that a glass is an ideal system to test this commonality [7]. Recently, Argon and Demkowicz performed molecular dynamics simulations to investigate plasticity in amorphous silicon (a-Si) [8]. These simulations reveal that the structure of a-Si consists of solid and liquidlike regions with fourfold and fivefold atomic coordinations, respectively. The liquidlike regions are found to locally facilitate plasticity through the nucleation of shear transformations. Shear transformations are also the mechanism of plasticity in metallic and polymeric glasses [8].

In this Letter, we present molecular dynamics (MD) simulation results for a single void in amorphous silica (a-SiO_2) subjected to a high shear rate between 10^9 and 10^{10} sec^{-1}. We prepared two a-SiO_2 systems using the melt-quench method [9]. The system sizes were $(25.64\ nm)^3$ with 1 118 817 atoms and $180.3 \times 296.7 \times 180.3\ nm^3$ with 633×10^6 atoms. The initial diameter of the void ranged between 3 and 50 nm, which covers nearly the entire range of void sizes observed in the damage zone in dynamic fracture simulations [10] and quasistatic stress corrosion cracking experiments [11] on silica glass. The interatomic potential in our simulations includes ionic and covalent effects through a combination of two-body and three-body terms [9], and it has been validated extensively by comparing the MD results for structural and mechanical properties of a-SiO_2 with experimental measurements and quantum mechanical calculations based on density functional theory [12].

The shear strain is applied with the Parrinello-Rahman approach in which the elements of a 3×3 matrix, spanned by the three vectors ($\boldsymbol{h}_1$, $\boldsymbol{h}_2$, $\boldsymbol{h}_3$) that describe the dimensions and shape of the MD box, are treated as dynamic variables [13]. Periodic boundary conditions are imposed, and the matrix ($\boldsymbol{h}_1$, $\boldsymbol{h}_2$, $\boldsymbol{h}_3$) evolves in time along with the atomic positions and velocities. The simulations were performed with temperature control [14] and also in the mi-

crocanonical ensemble. We find the same results for void deformation, damage, and breakup in these ensembles.

Figure 1(a) is a snapshot of a deformed void at a shear strain of 15% in silica glass at room temperature. The initial diameter of the void is 10 nm. As the strain increases, so does the void deformation, and damage in the form of nanocracks nucleates on the void surface. The same kind of deformation and damage is also observed for voids of initial diameters 3 and 50 nm. Stress calculations [15] reveal that nanocracks form along the direction of the maximum tensile stress. Joseph has proposed a cavitation criterion in a flowing liquid, according to which a cavity nucleates in the direction of maximum tensile stress much like the way fracture occurs in amorphous solids [7]. In the case of a Newtonian fluid in pure shear, the cavitation direction is predicted to be 45° from the shear plane. This is indeed the direction of nanocrack initiation on void surfaces in our simulations.

Figure 1(b) shows the strain variation of the deformation parameter D for initially spherical voids of diameters 3 (blue), 10 (red), and 50 nm (green). In all three cases, D increases linearly with strain up to $\varepsilon = 15\%$, which is an indication that the void deformation is elastic. To distinguish between elastic and plastic void deformations, we switch off the shear strain after it reaches a certain value and let the system relax without shear. We find that if the shear strain rate is dropped to zero before the strain reaches 15%, voids recover their initial spherical shapes and sizes. Furthermore, there is no damage around the voids for strains less than 15%. Plastic deformation appears for shear strain $\varepsilon > 15\%$, and around $\varepsilon = 25\%$ the voids begin to deform into threadlike structures with nanocracks on their surfaces. Plastic deformation of voids into threadlike structures is consistent with the continuum-based theory [5]. This is due to the fact that the capillary number C in MD simulations is very large, which is the condition for the validity of the continuum theory. Based on the MD simulation results for the surface tension γ and viscosity μ, our estimate for the critical value of C $(= Ga\mu/\gamma)$ at a strain of 25% is 10^{13} [16]. At this strain, threefold-coordinated silicon and nonbridging oxygen defects are formed as a result of broken Si-O bonds.

Figures 2(a) and 2(b) are snapshots showing long, thin voids with nanocracks on the surfaces near the middle of the long axis. Initially, these were spherical voids of diameters 3 and 50 nm. In both cases, the voids become threadlike before breakup, which occurs above a strain of 40%. Figure 2(c) shows plastic deformation of a void, which was initially a sphere of diameter 10 nm. The snapshot taken at $\varepsilon = 35\%$ shows a long, thin void with ends deformed roughly like an S shape. There are nanocracks on the surface and near the ends of the void. As time evolves, nanocracks grow and the void becomes more elongated, and at $\varepsilon = 40\%$ the void fragments; see Fig. 2(d).

To confirm that the void deformation is indeed plastic in the nonlinear deformation regime, we have performed several simulations in which we switch off the shear strain after it exceeds 15% and let the system evolve without any external strain. We find that neither the nanocracks nor the pointed ends heal completely in such strain-free systems. When the shear is turned off in the case of the S-shaped void, the pointed ends fragment in a manner akin to the "end-pinching" mechanism of drop breakup in fluids [2,17,18]. Note that Hinch and Acrivos [6] predicted an S-shaped drop in the limit $\lambda \ll 1$ and $C \gg 1$, and experiments on bubbles in viscous liquids in simple shear flow support their theoretical analysis based on the slender-body theory [2]. Threadlike deformations of inviscid drops have also been observed experimentally in fluids under high shear rates [2,17].

Detailed analyses of elastic-to-plastic void deformation and crack initiation and growth reveal a novel mechanism involving strain-enhanced defect transport; see Figs. 3(a)–3(c). In the unstrained a-SiO_2, each Si atom (yellow) is connected to four O atoms (red) in the form of a SiO_4 tetrahedron, and these tetrahedra are linked into nanometer size —Si–O–Si–O— rings through corner-sharing O atoms. In Fig. 3(a), green and blue regions represent 6- and 9-membered rings, respectively, at a strain of 5%. The magenta atom is a bridging O, and the blue atom is a threefold-coordinated Si atom in the 9-membered ring. Figure 3(b) shows that at a strain of 8% the magenta

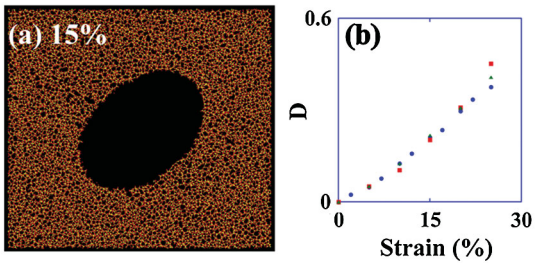

FIG. 1 (color). (a) Shear deformation of a spherical void of diameter 10 nm. (b) Strain variation of the deformation parameter D [$= (L - B)/(L + B)$] for voids of initial diameters 3 (blue circles), 10 (red squares), and 50 nm (green triangles).

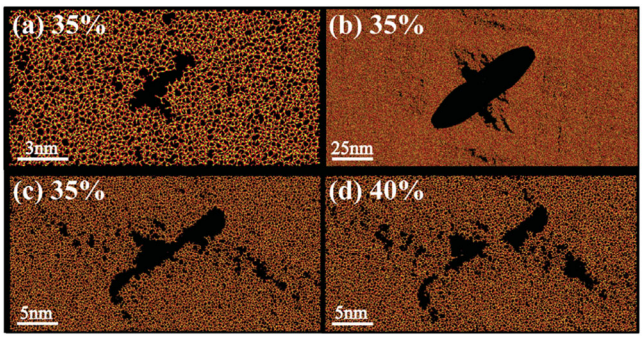

FIG. 2 (color). Panels (a) and (b) show plastic deformations of voids of initial diameters 3 and 50 nm, respectively. Panel (c) shows a plastically deformed void which was initially a sphere of diameter 10 nm, and panel (d) shows its breakup at $\varepsilon = 40\%$.

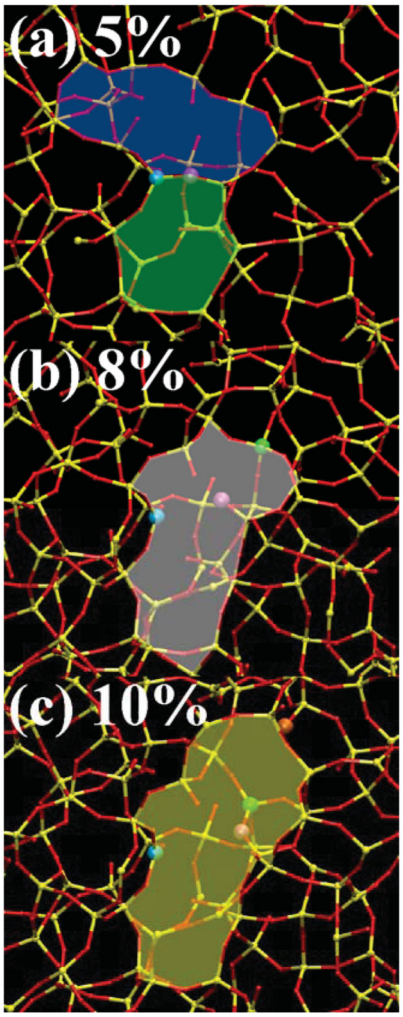

FIG. 3 (color). Point defects responsible for shear deformation and flow and crack nucleation in silica glass. (a) A 6-membered —Si–O–Si–O— ring (green) adjacent to a 9-membered ring (blue) with a fully coordinated O (magenta) and a threefold-coordinated Si defect (blue). (b) At a strain of 8%, the magenta O atom becomes nonbridging, and the blue Si atom remains undercoordinated. These point defects reside on a 13-membered ring (gray). (c) At a strain of 10%, the green Si and magenta O atoms become fully coordinated by bonding with each other, but the blue Si is still undercoordinated. The yellow region is inside a 14-membered ring.

O atom becomes nonbridging, while the blue Si atom remains undercoordinated. The gray ring with these Si and O defects is a 13-membered ring. At a strain of 10%, the green Si and magenta O atoms become fully coordinated by bonding with each other. The blue Si is still undercoordinated but now belongs to a 14-membered ring (yellow). Nonbridging oxygen and threefold-coordinated silicon atoms play pivotal roles in the nucleation of cracks through the enlargement of —Si–O–Si–O— rings and in void deformation and shear flow in silica glass.

Figure 4(a) shows the time variation of the density of undercoordinated Si and O defects in a region, which encloses the deformed void (initial diameter 3 nm) and the damage zone around it. We find that this region has approximately the same number of threefold-coordinated Si and nonbridging O atoms. The defect density remains small for $\varepsilon < 15\%$ and then increases before leveling off as steady plastic flow is established in the system. Voids break up as soon as the defect density saturates. Figure 4(b) shows the Si-O pair-distribution function $g(r)$ for defects when the void is elastically deformed ($\varepsilon = 15\%$) and after it breaks up ($\varepsilon = 55\%$). In both cases, there is only one prominent peak at 1.57 Å, which is shifted to the left relative to the first peak in the $g_{\text{Si-O}}(r)$ in bulk a-SiO_2 (1.62 Å) because the defects are undercoordinated. The peak height drops significantly after the system undergoes elastic-to-plastic transformation. We have also investigated the dynamics of these defects and find steady plastic flow along the shear direction. Perpendicular to the direction of shear flow, the mean square displacement for these defects oscillates in the elastic regime but increases linearly with time after the plastic flow is established. The diffusion coefficient for defects in the plastic regime is $\sim 10^{-5}$ cm^2/s, which is typical of liquids.

Mott has proposed a model for viscosity of a-SiO_2, which is based on the motion of defects on —Si–O–Si–O— rings [19]. In this model, two kinds of defects are invoked to explain experimental results on plastic flow: (a) a threefold-coordinated Si atom and a nonbridging oxygen atom arising from a single broken bond and (b) breaking of a pair of bonds in close proximity and recombination of resulting threefold-coordinated Si and nonbridging O atoms. In our simulations, we observe both kinds of defects in shear-induced plastic flow in silica glass.

We have also investigated changes in the void shape and elastic-to-plastic transition in silica glass at 1200 K. The high temperature systems were prepared by heating room temperature silica glass to 600, 900, and 1200 K. At each intermediate temperature and at 1200 K, the systems were well thermalized before subjecting them to shear strain. The applied stains rates were the same as at room temperature. We observe that the voids at 1200 K are partially filled with atoms released from the void surfaces [see Fig. 5(a)], which was not the case at room temperature [compare with

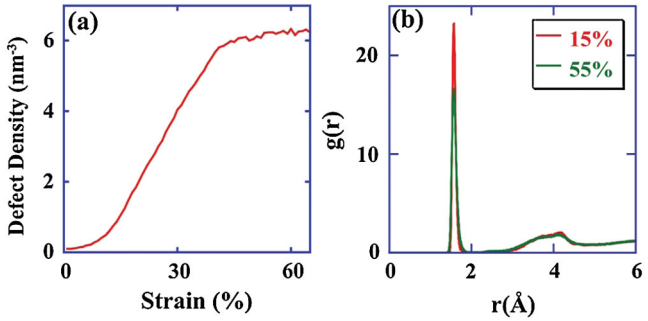

FIG. 4 (color). (a) Density of Si and O defects in the damage zone as a function of strain and (b) Si-O pair-distribution function for these defects. The initial void diameter was 3 nm.

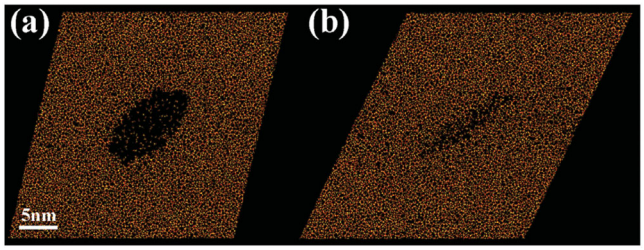

FIG. 5 (color). Panels (a) and (b) show void deformation and thinning of the void at $\varepsilon = 22\%$ and 44%, respectively. Here the temperature is 1200 K. As the strain is increased, the void shape changes from spherical to ellipsoidal and then becomes threadlike before the void breaks up.

Fig. 1(a)]. At 1200 K, the density of atoms inside the voids increases with time. The voids still undergo spherical-to-ellipsoidal shape transformation [Fig. 5(a)], but the time variation of the deformation parameter is slightly less than that at room temperature. Voids deform into long ellipsoidal shapes with pointed ends, and their breakup is again preceded by threadlike structures just as at room temperature; see Fig. 5(b).

In conclusion, MD simulations reveal that, despite the enormous differences in spatiotemporal scales, the observed shape changes and fragmentation of voids in silica glass are remarkably similar to the deformation and breakup of macroscopic inviscid drops at high shear rates. For small shear strain (<15%), spherical voids in silica glass deform elastically into ellipsoids. At larger strains, nanocracks appear on void surfaces, and voids deform plastically into threadlike structures before fragmenting at a strain of ~40%. We have also observed void deformation that resembles an S-shaped bubble in a sheared liquid. Finally, our simulations reveal that the underlying mechanisms of shear-induced void deformation, damage, and flow in silica glass involves Si-O bond breaking and the migration of threefold-coordinated silicon and nonbridging oxygen atoms on —Si–O–Si–O— rings.

This work was supported by DOE-SciDAC and NSF-ITR grants. Simulations were performed on the 6120-processor Linux cluster at USC's Research Computing Facility and on the 2048-processor Linux cluster at our Collaboratory for Advanced Computing and Simulations. We thank Dr. Lin Yang for validating our interatomic potential with quantum mechanical calculations.

[1] A. Acrivos, Ann. N.Y. Acad. Sci. **404**, 1 (1983).
[2] H. Stone, Annu. Rev. Fluid Mech. **26**, 65 (1994).
[3] J. M. Rallison, Annu. Rev. Fluid Mech. **16**, 45 (1984).
[4] M. Manga, J. Castro, K. V. Cashman, and M. Loewenberg, J. Volcanol. Geotherm. Res. **87**, 15 (1998).
[5] E. J. Hinch and A. Acrivos, J. Fluid Mech. **91**, 401 (1979).
[6] E. J. Hinch and A. Acrivos, J. Fluid Mech. **98**, 305 (1980).
[7] D. Joseph, J. Fluid Mech. **366**, 367 (1998).
[8] A. S. Argon and M. J. Demkowicz, Metall. Mater. Trans. A **39**, 1762 (2008).
[9] P. Vashishta, R. K. Kalia, J. P. Rino, and I. Ebbsjo, Phys. Rev. B **41**, 12 197 (1990).
[10] C. L. Rountree, R. K. Kalia, E. Lidorikis, A. Nakano, L. Van Brutzel, and P. Vashishta, Annu. Rev. Mater. Res. **32**, 377 (2002).
[11] F. Célarié, S. Prades, D. Bonamy, L. Ferrero, E. Bouchaud, C. Guillot, and C. Marlière, Phys. Rev. Lett. **90**, 075504 (2003).
[12] Validation of the interatomic potential is provided by quantum mechanical calculations based on the density functional theory (DFT) using a plane-wave pseudopotential method in conjunction with a parameter-independent generalized gradient approximation for the exchange-correlation potential. A 192-atom a-SiO_2 system was prepared with a MD simulation and relaxed with the DFT method. The excellent agreement in the network topology of a-SiO_2 between DFT and MD simulations validates the high quality of the interatomic potential for SiO_2. More importantly, the forces on Si and O atoms calculated from DFT and MD simulations for the same a-SiO_2 configuration deviate less than 4.5% and 6%, respectively. (DFT calculations were performed by L. Yang at Lawrence Livermore National Laboratory.)
[13] M. Parrinello and A. Rahman, Phys. Rev. Lett. **45**, 1196 (1980).
[14] H. J. C. Berendsen, J. P. M. Postma, W. F. Vangunsteren, A. Dinola, and J. R. Haak, J. Chem. Phys. **81**, 3684 (1984).
[15] K. S. Cheung and S. Yip, J. Appl. Phys. **70**, 5688 (1991).
[16] We calculate the surface tension from Griffith's energy relation $\gamma = \frac{(1-\nu^2)K_{1c}^2}{2E}$ under the plane-strain condition using our MD simulation results for the Poisson's ratio ($\nu = 0.22$), Young's modulus ($E = 67$ GPa), and stress intensity factor for a mode I fracture ($K_{1c} = 1$ MPa $m^{1/2}$); see K. Nomura *et al.*, J. Phys. D (to be published). Our results are in good agreement with experimental values: $\nu = 0.197$ and $E = 69.1$ GPa [Q. Wang *et al.*, J. Non-Cryst. Solids **143**, 65 (1992)]; $K_{1c} = 0.8$–1.2 MPa $m^{1/2}$ [see R. K. Kalia *et al.*, Int. J. Fract. **121**, 71 (2003) and also J. P. Lucas *et al.*, Scr. Metall. Mater. **32**, 743 (1995)]. The viscosity at a strain of 25% is estimated from Eq. (2) in Ref. [19] with the knowledge of the density of defects [Fig. 4(a)] and our estimates for the diffusion coefficient (10^{-9} m^2/s) and the energy needed to form such a defect (~1 eV) at that strain. With these values of γ and μ, the critical value of C is 10^{13} for the 3 nm size void at a strain rate of 10^9 sec^{-1}.
[17] G. I. Taylor, Proc. R. Soc. A **138**, 41 (1932).
[18] H. P. Grace, Chem. Eng. Commun. **14**, 225 (1982).
[19] N. F. Mott, Philos. Mag. B **56**, 257 (1987).